IEEE Access
Multidisciplinary | Rapid Review | Open Access Journal

Received November 16, 2020, accepted December 14, 2020, date of publication December 17, 2020,
date of current version December 31, 2020.

Digital Object Identifier 10.1109/ACCESS.2020.3045606

Adaptive Integral-Sliding-Mode Control for Spacecraft Single-Axis Pointing Using Two Torques

TAO WANG[1,2] AND YINGCHUN ZHANG[1]
[1]School of Astronautics, Harbin Institute of Technology, Harbin 150001, China
[2]China Academy of Space Technology, Beijing 100094, China

Corresponding author: Tao Wang (15210004024@163.com)

ABSTRACT This paper deals with the attitude control problem of a nearly axis-symmetric spacecraft actuated by two torques perpendicular to its symmetry axis. As a result, the spacecraft symmetry axis is unactuated and the rotation about it is uncontrollable. Our objective aims to stabilize the symmetry axis to an arbitrary inertial direction irrespective of the spinning motion about it. First, a non-smooth controller is derived via homogeneous techniques to align the symmetry axis in finite time when there are no uncertainties. To compensate for perturbations induced by uncertain inertias, unknown external disturbances and actuator faults, an adaptive integral sliding mode controller is developed by combining adaptive control and integral sliding modes with the non-smooth controller. The resultant adaptive controller can stabilize the system states into a small neighborhood around the sliding mode. Consequently, the performance of the non-smooth controller can be approximately recovered, even in the presence of uncertainties, which ensures significant robustness and high control accuracy. Numerical examples are presented to verify the effectiveness and advantages of the proposed methods.

INDEX TERMS Adaptation, fault tolerance, finite-time, integral sliding modes, axis-symmetric spacecraft, spin-axis stabilization, two torques.

I. INTRODUCTION

The attitude motion of a rigid spacecraft has 3 degrees-of-freedom and it becomes underactuated when the available control torques are fewer than three. The attitude control of underactuated spacecraft has attracted increasing attention of researchers because it can provide significant tolerance to partial actuator failures, as occurred in the Dawn spacecraft and the Kepler telescope [1], [2], and greatly improve the reliability of the attitude control system.

Many studies have considered the attitude control of spacecraft underactuated by internal torques, such as reaction wheels and control moment gyros [3]. In this case, the angular momentum conservation constraint is a critical challenge and various approaches have been proposed to handle it and meanwhile achieve single-axis pointing [4], [5], three-axis attitude stabilization [6]–[11] or tracking control [12].

In contrast, the spacecraft underactuated by external torques, such as reaction thrusters, does not have the momentum conservation problem and its attitude control is generally addressed from two perspectives. The first seeks discontinous or time-varying control laws to achieve three-axis attitude stabilization [13]–[19] when the system is fully controllable, for example, when only two external control torques are available and the spacecraft is asymmetric, or when the spacecraft is axis-symmetric and the torques are not normal to the symmetry axis [20], [21]. The second perspective aims to stabilize a reduced yet fully controllable subsystem of the original uncontrollable system. For example, if the spacecraft is axis-symmetric and the two torques are perpendicular to the symmetry axis, the rotation about the symmetry axis is not controllable. In addition, it is common that the uncontrollable symmetry axis has nonzero angular velocity for on-orbit spacecraft. To deal with this scenario, spin-axis stabilization was proposed to stabilize the symmetry axis of the spacecraft to an arbitrary target inertial direction irrespective of the spinning motion about the symmetry axis [22]–[24]. Such type of attitude control can have practical applications when the spacecraft symmetry axis is a normal vector of the solar panel, or the line-of-sight

The associate editor coordinating the review of this manuscript and approving it for publication was Youqing Wang.

of an antenna, a telescope or a camera, etc. For these cases, the main concern is to align the line-of-sight of the spacecraft along the target direction while the rotation motion about it is irrelevant.

Tsiotras and Longuski [22], Tsiotras [23] first derived proportional-derivative feedback laws asymptotically stabilizing the spinning axis of an axis-symmetric spacecraft with two torques. In spite of their remarkable simplicity, these algorithms have poor robustness against inertia uncertainties and external disturbances. For better robustness, a spin-stabilization law was developed in [25] by means of the internal modal principle to reject sinusoidal disturbances with known frequencies. A computational $\mathcal{H}_\infty$ feedback law was designed in [26] to point the spacecraft symmetry axis while suppressing the influence of unknown disturbances. Neither of the designs in [25], [26] considered the inertia uncertainties. A more recent work by [27] presented an adaptive sliding mode controller for spin-stabilization with significantly improved robustness to system uncertainties. The studies in [14], [22], [23], [26], [27] all utilized the (w, z)-coordinate to describe the spacecraft attitude. The resultant attitude kinematics have the appealing feature that the rotation of the symmetry axis is decoupled from the rotation about it, and therefore significantly facilitates spin-stabilization law design for axis-symmetric spacecraft.

None of spin-stabilization laws derived in [14], [22], [23], [25]–[27] consider the influence of uncertain inertia, unknown disturbances, and actuator faults all together. In addition, they are all asymptotically convergent. Compared to asymptotic controllers, finite-time control methods ensure convergence in finite time and hence faster convergence speed and better robustness to uncertainties. Typical finite-time control design methods include homogeneous theory, adding a power integrator techniques, terminal sliding modes [28], and higher-order sliding modes [29], [30]. Various finite-time attitude control laws were designed for fully actuated spacecraft [31]–[34]. Recently, finite-time angular velocity observers were designed in [18], [19] and then used to obtain velocity-free three-axis attitude stabilization laws with two torques. The combined observer-controller, however, ensures local asymptotic stability instead of finite-time stability. Therefore, the finite-time attitude control of spacecraft with two torques still needs further research.

This paper investigates the spin-axis stabilization of an axis-symmetric spacecraft controlled by two external torques normal to the symmetry axis. The symmetry axis is also the spinning axis that is required to point to a desired inertial direction. A Hölder-continuous controller with a nonlinear proportional-derivative structure is designed by means of the homogeneous theory to stabilize the spinning axis to the target direction in finite time, when there is no system uncertainties. It is then developed into an adaptive controller with significant robustness against uncertain inertia, unknown external disturbances, and actuator faults by combining integral sliding mode (ISM) methods and adaptive techniques. The main contributions of the paper are twofold.

1) The ISM surface is designed such that the sliding motion evolves exactly as the uncertainty-free closed-loop system under the Hölder-continuous controller. In other words, on the sliding mode the spinning axis of the spacecraft will converge to the target direction in finite time. As a result, the parameter tuning for the proposed ISM is greatly simplified because it is similar to that for the Hölder-continuous controller and has a clear physical meaning.
2) The proposed adaptive ISM controller can actively estimate and compensate for system uncertainties such as uncertain inertia, unknown external disturbances and actuator faults in real time. As a result, the performance of the Hölder-continuous controller can be approximately recovered even in the presence of unknown perturbations, and the spacecraft spinning axis can be pointed to the target direction with high precision. Numerical examples are presented to demonstrate the effectiveness and advantages of the proposed methods compared to the existing spin-stablization controllers derived in [25], [27].

This paper proceeds as follows: Section II presents some useful lemmas and the attitude equations of a nearly axis-symmetric spacecraft actuated by two torques. In section III, a Hölder-continuous controller is designed when there are no uncertainties, and then developed into an adaptive ISM controller, to stabilize the spacecraft symmetry axis to any inertial direction. Numerical examples are given in Section IV and conclusions are summarized in Section V.

II. PRELIMINARIES

In the following, denote by $\boldsymbol{I}_n$ the n-by-n identity matrix, $\mathbf{0}_n = [0, \ldots, 0]^T \in \mathbb{R}^n$, $\mathbf{0}_{n\times n}$ the n-by-n zero matrix, and $\mathbb{I}_n$ the index set $\{1, \ldots, n\}$. For any $x \in \mathbb{R}$ and $\alpha \geq 0$, define the power functions $\mathrm{sgn}^\alpha(x) = \mathrm{sgn}(x)|x|^\alpha$ and $\mathrm{sat}_\alpha(x) = \mathrm{sgn}(x)\min\{|x|^\alpha, 1\}$, where $\mathrm{sgn}(\cdot)$ is the standard sign function. It can be seen that $\mathrm{sgn}^\alpha(x)$ is a continuous non-smooth function when $0 < \alpha < 1$, and $\mathrm{sat}_\alpha(x)$ becomes the standard saturation function $\mathrm{sat}(x)$ when $\alpha = 1$. For $\boldsymbol{x} = [x_1, \cdots, x_n]^T \in \mathbb{R}^n$ and $\alpha \geq 0$, define $\mathrm{sgn}^\alpha(\boldsymbol{x}) = [\mathrm{sgn}^\alpha(x_1), \ldots, \mathrm{sgn}^\alpha(x_n)]$ and $\mathrm{sat}_\alpha(\boldsymbol{x}) = [\mathrm{sat}_\alpha(x_1), \ldots, \mathrm{sat}_\alpha(x_n)]$. Denote by $\|\cdot\|$ the Euclidean norm of a vector and the induced 2-norm of a matrix.

A. FINITE-TIME STABILITY

Consider the system

$$\dot{\boldsymbol{x}} = \boldsymbol{f}(\boldsymbol{x}), \quad \boldsymbol{f}(\mathbf{0}_n) = \mathbf{0}_n, \ \boldsymbol{x} \in \mathbb{R}^n \tag{1}$$

where $\boldsymbol{f} : \boldsymbol{x} \in V \mapsto [f_1(\boldsymbol{x}), \cdots, f_n(\boldsymbol{x})]^T \in \mathbb{R}^n$ is continuous on an open neighborhood V of the origin. System (1) is finite-time stable if it is Lyapunov stable and every solution $\boldsymbol{x}(t, \boldsymbol{x}_0)$ starting from any initial condition $\boldsymbol{x}_0 \in V$ converges to the origin in a finite time $T(\boldsymbol{x}_0) \geq 0$.

Definition 1: Consider system (1) and denote by U a neighborhood of $\boldsymbol{x} = \mathbf{0}_n$. The origin of system (1) is said to be finite-time stable if it is 1) Lyapunov stable in U and

2) finite-time convergent in U, that is, for any initial condition $\boldsymbol{x}_0 \in U$ there exists a time $T(\boldsymbol{x}_0) \geq 0$ such that the solution satisfies $\lim_{t\to T(\boldsymbol{x}_0)} \boldsymbol{x}(\boldsymbol{x}_0, t) = \boldsymbol{0}_n$. If $U = \mathbb{R}^n$, then the origin is globally finite-time stable.

Given $\lambda > 0$ and a weight vector $\boldsymbol{r} = [r_1, \cdots, r_n]^T \in \mathbb{R}^n$, define a dilation operator $\Delta_\lambda^r : \mathbb{R}^n \mapsto \mathbb{R}^n$ as $\Delta_\lambda^r \boldsymbol{x} = [\lambda^{r_1} x_1, \cdots, \lambda^{r_n} x_n]^T$, where $\boldsymbol{x} = [x_1, \cdots, x_n]^T \in \mathbb{R}^n$. Then, system (1), or equivalently the vector field $\boldsymbol{f}(\boldsymbol{x})$ is said to be homogeneous of degree $l \in \mathbb{R}$ with respect to the dilation Δ_λ^r if $f_i(\Delta_\lambda^r \boldsymbol{x}) = \lambda^{r_i+l} f_i(\boldsymbol{x})$ for any $i \in \mathbb{I}_n$, $\boldsymbol{x} \in V$, and $\lambda > 0$, and l satisfies $l > -\min\{r_1, \cdots, r_n\}$. The following result has been proven in [35].

Lemma 1: Consider the following continuous system

$$\dot{\boldsymbol{x}} = \boldsymbol{f}(\boldsymbol{x}) + \hat{\boldsymbol{f}}(\boldsymbol{x}), \quad \boldsymbol{x} \in \mathbb{R}^n \tag{2}$$

where $\boldsymbol{f}(\boldsymbol{0}_n) = \hat{\boldsymbol{f}}(\boldsymbol{0}_n) = \boldsymbol{0}_n$. Assume that the unperturbed system $\dot{\boldsymbol{x}} = \boldsymbol{f}(\boldsymbol{x})$ is homogeneous of degree $l < 0$ with respect to a dilation Δ_λ^r and is asymptotically stable. Then, the origin of system (1) is locally finite-time stable if

$$\lim_{\lambda\to 0} \frac{f_i(\Delta_\lambda^r \boldsymbol{x})}{\lambda^{r_i+l}} = 0, \quad \forall \boldsymbol{x} \neq \boldsymbol{0}_n, \ \forall i \in \mathbb{I}_n. \tag{3}$$

System (2) is globally finite-time stable if it is globally asymptotically stable and locally finite-time stable.

B. SYSTEM EQUATIONS

Consider a rigid spacecraft attached with a body frame $\mathcal{F}_B = \{\hat{\boldsymbol{b}}_1, \hat{\boldsymbol{b}}_2, \hat{\boldsymbol{b}}_3\}$, where $\hat{\boldsymbol{b}}_i$, $i = 1, 2, 3$, are orthogonal unit vectors representing the coordinate axes. Denote by $\mathcal{F}_I = \{\hat{\boldsymbol{i}}_1, \hat{\boldsymbol{i}}_2, \hat{\boldsymbol{i}}_3\}$ the inertial frame. Letting $[-a, -b, c]^T \in \mathbb{R}^3$ be the direction cosines of $\hat{\boldsymbol{b}}_3$ in $\mathcal{F}_I$, the attitude of $\mathcal{F}_B$ relative to $\mathcal{F}_I$ can be parameterized by means of the (w, z)-coordinates with [36]

$$w_1 = \frac{b}{1+c}, \quad w_2 = \frac{-a}{1+c}$$

and $z \in \mathbb{R}$ being a rotation angle about $\hat{\boldsymbol{i}}_1$. The attitude kinematics in terms of (w, z)-coordinates and the Euler dynamics of the spacecraft are given by [36]

$$\begin{aligned}
\dot{w}_1 &= \Omega_3 w_2 + \Omega_2 w_1 w_2 + \Omega_1 \frac{1 + w_1^2 - w_2^2}{2} \\
\dot{w}_2 &= -\Omega_3 w_1 + \Omega_1 w_1 w_2 + \Omega_2 \frac{1 + w_2^2 - w_1^2}{2} \\
\dot{z} &= \Omega_3 - \Omega_1 w_2 + \Omega_2 w_1 \\
\boldsymbol{J}\dot{\boldsymbol{\Omega}} &= -\boldsymbol{\Omega} \times \boldsymbol{J}\boldsymbol{\Omega} + \boldsymbol{E}(t)\boldsymbol{\tau} + \boldsymbol{d}
\end{aligned} \tag{4}$$

where $\boldsymbol{\Omega} = [\Omega_1, \Omega_2, \Omega_3]^T \in \mathbb{R}^3$ is the spacecraft angular velocity expressed in $\mathcal{F}_B$, $\boldsymbol{J} \in \mathbb{R}^{3\times 3}$ is the spacecraft inertia matrix, $\boldsymbol{\tau} \in \mathbb{R}^3$ is the control torque, and $\boldsymbol{d} \in \mathbb{R}^3$ denotes the external disturbance torque. $\boldsymbol{E}(t) = \text{diag}\{e_1(t), e_2(t), e_3(t)\}$ is the health indicator matrix of the actuators with $0 \leq e_i(t) \leq 1$, $i = 1, 2, 3$. In particular, $e_i(t) = 1$ means that the ith actuator is completely health and can produce control torques as commanded. $0 < e_i(t) < 1$ means that the ith actuator encounters the fault of fading control torques while $e_i(t) = 0$ corresponds to the case that the ith actuator completely fails.

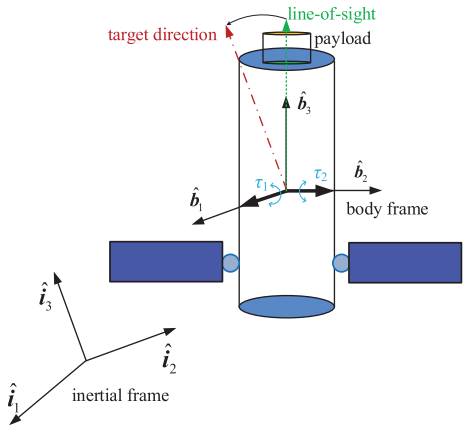

FIGURE 1. Reference frames for an axis-symmetric spacecraft.

As shown in Fig. 1, we assume in the following that the spacecraft is nearly axis-symmetric and only two torques perpendicular to the symmetry axis are available for control, i.e., $0 < e_1(t), e_2(t) \leq 1$ and $e_3(t) = 0$ for all $t \geq 0$. Without loss of generality, let the body axes $\{\hat{\boldsymbol{b}}_1, \hat{\boldsymbol{b}}_2, \hat{\boldsymbol{b}}_3\}$ align with the principal axes of the spacecraft, and $\hat{\boldsymbol{b}}_3$ along the unactuated symmetry axis. In other words, $\boldsymbol{J} = \text{diag}\{J_1, J_2, J_3\}$ and $\boldsymbol{\tau} = [\tau_1, \tau_2, 0]^T$. The control objective is to point the symmetry axis $\hat{\boldsymbol{b}}_3$ to a target direction fixed in the inertial space irrespective of the spinning motion about $\hat{\boldsymbol{b}}_3$. Note that the target direction can be an arbitrary direction in the inertial space. Note that the choice of the inertial frame is very flexible. We can always choose an inertial frame such that $\hat{\boldsymbol{i}}_3$ coincides with the target direction. Therefore, the objective can, without loss of generality, reduce to stabilizing the symmetry axis $\hat{\boldsymbol{b}}_3$ to $\hat{\boldsymbol{i}}_3$.

Note that w_1 and w_2 now describe the direction of the symmetric axis $\hat{\boldsymbol{b}}_3$ in the inertial space and $\hat{\boldsymbol{b}}_3$ is aligned with $\hat{\boldsymbol{i}}_3$ if and only if $w_1 = w_2 = 0$. The equations governing the evolution of $\hat{\boldsymbol{b}}_3$ can be derived as [27]

$$\dot{\boldsymbol{w}} = \boldsymbol{S}(\Omega_3)\boldsymbol{w} + \boldsymbol{F}(\boldsymbol{w})\boldsymbol{\Omega}_{12} \tag{5}$$

$$\boldsymbol{J}_{12}\dot{\boldsymbol{\Omega}}_{12} = \boldsymbol{J}_a \boldsymbol{S}(\Omega_3)\boldsymbol{\Omega}_{12} + \boldsymbol{E}_{12}(t)\boldsymbol{\tau}_{12} + \boldsymbol{d}_{12} \tag{6}$$

where $\boldsymbol{\Omega}_{12} = [\Omega_1, \Omega_2]^T$, $\boldsymbol{J}_{12} = \text{diag}\{J_1, J_2\}$, $\boldsymbol{J}_a = \boldsymbol{J}_{12} - J_3\boldsymbol{I}_2$, $\boldsymbol{E}_{12}(t) = \text{diag}\{e_1(t), e_2(t)\}$, $\boldsymbol{\tau}_{12} = [\tau_1, \tau_2]^T$ and $\boldsymbol{d}_{12} = [d_1, d_2]$; $\boldsymbol{S}(\Omega_3)$ is a skew-symmetric matrix given by

$$\boldsymbol{S}(\Omega_3) = \begin{bmatrix} 0 & \Omega_3 \\ -\Omega_3 & 0 \end{bmatrix}$$

and $\boldsymbol{F}(\boldsymbol{w})$ is a symmetric matrix given by

$$\boldsymbol{F}(\boldsymbol{w}) = \frac{1}{2}[(1 - \boldsymbol{w}^T\boldsymbol{w})\boldsymbol{I}_2 + 2\boldsymbol{w}\boldsymbol{w}^T].$$

Since the spacecraft is nearly axis-symmetric about $\hat{\boldsymbol{b}}_3$, it follows that $J_1 = J_2$ and $\Omega_3(t) = \Omega_3(0) + \int_0^t d_3(\phi)/J_3 \mathrm{d}\phi$. Evidently, $\Omega_3(t) = \Omega_3(0)$ if $d_3(t) = 0$ for all $t \geq 0$. The angular velocity along the other two axes will not affect the symmetry axis. In other words, the angular velocity

about the symmetry axis remains constant if the disturbance torque along $\hat{\boldsymbol{b}}_3$ is always zero, and is time-varying otherwise.

The reduced system given in (5) and (6) completely describes the evolution of the symmetry axis $\hat{\boldsymbol{b}}_3$ in 3-dimensional space. It has two degrees-of-freedom and two control inputs, and, therefore, is a fully actuated system.

Assumption 1: The spacecraft is nearly axis-symmetric and its inertia is constant.

Assumption 2: There exists a constant $\delta_\omega \geq 0$ such that the angular velocity along $\hat{\boldsymbol{b}}_3$ is bounded as $|\Omega_3(t)| \leq \delta_\omega$.

Assumption 3: There exists a constant $\delta_d \geq 0$ such that $\|\boldsymbol{d}_{12}\| \leq \delta_d$.

Assumption 4: There exists a constant $0 \leq \chi_e < 1$ such that $\|\boldsymbol{I}_2 - \boldsymbol{E}_{12}(t))\| \leq \chi_e$ and $\chi_e + \|\Delta \boldsymbol{J}_{12}\boldsymbol{J}_{12}^{-1}\| < 1$ for all $t \geq 0$.

Assumptions 1-3 are reasonable for realistic spacecraft and also adopted in [27]. Assumption 4 means that the perturbations induced by actuator faults and inertia uncertainties cannot be arbitrarily large in order to attain effective attitude control. The remaining control authority of the actuators needs to be able to suppress the perturbing effect, which is also reasonable.

III. CONTROLLER DESIGN

In this section, we aim to design control laws that can point the unactuated spinning axis $\hat{\boldsymbol{b}}_3$ to an arbitrary inertial direction even in the presence of the above uncertainties. This objective is attained by stabilizing the reduced system given in (5) and (6) to the origin or a small neighborhood of the origin. Note that the global stability or global convergence discussed in the following refers to the behavior of the reduced states, i.e., $(\boldsymbol{w}, \boldsymbol{\Omega}_{12})$, instead of the 6-dimensional states of the full attitude motion system given in (4), i.e., $(\boldsymbol{w}, z, \boldsymbol{\Omega})$.

A. FINITE-TIME CONTROLLER WITHOUT UNCERTAINTIES

First, the uncertainty-free case is considered. Assume that the external disturbance is zero (i.e., $\boldsymbol{d} = \boldsymbol{0}_3$), the 1st and 2nd actuators are fully healthy ($\boldsymbol{E}_{12}(t) = \boldsymbol{I}_2$) and the spacecraft model is precisely known. The following simple nonlinear controller is designed

$$\boldsymbol{\tau}_{12}^* = -\frac{k_1}{\sqrt{1+\|\boldsymbol{w}\|^2}}\frac{\boldsymbol{w}}{\|\boldsymbol{w}\|^{1-\alpha_1}} - k_2 \mathrm{sat}_{\alpha_2}(\boldsymbol{\Omega}_{12}) \tag{7}$$

where $k_1, k_2 > 0$, $0 < \alpha_1 < 1$, and $\alpha_2 = 2\alpha_1/(1+\alpha_1)$. One can verify

$$\lim_{\|\boldsymbol{w}\|\to 0} \frac{\boldsymbol{w}}{\|\boldsymbol{w}\|^{1-\alpha_1}} = \boldsymbol{0}_2$$

which implies that $\boldsymbol{\tau}_{12}^*$ is continuous with respect to $\boldsymbol{w}$ and $\boldsymbol{\Omega}_{12}$. In addition, it follows from $\|\boldsymbol{w}\|^{\alpha_1}/\sqrt{1+\|\boldsymbol{w}\|^2} \leq 1$ and $\|\mathrm{sat}_{\alpha_2}(\boldsymbol{\Omega}_{12})\| \leq \sqrt{2}$ that $\boldsymbol{\tau}_{12}^*$ is bounded as

$$\|\boldsymbol{\tau}_{12}^*\| \leq k_1 + \sqrt{2}k_2. \tag{8}$$

Letting $\boldsymbol{\tau}_{12} = \boldsymbol{\tau}_{12}^*$ and substituting (7) into (6) yields

$$\boldsymbol{J}_{12}\dot{\boldsymbol{\Omega}}_{12} = \boldsymbol{J}_a\boldsymbol{S}(\Omega_3)\boldsymbol{\Omega}_{12} - \frac{k_1}{\sqrt{1+\|\boldsymbol{w}\|^2}}\frac{\boldsymbol{w}}{\|\boldsymbol{w}\|^{1-\alpha_1}} - k_2\mathrm{sat}_{\alpha_2}(\boldsymbol{\Omega}_{12}). \tag{9}$$

The following theorem states that the closed-loop trajectory $(\boldsymbol{w}(t), \boldsymbol{\Omega}_{12}(t))$ converges to zero in finite time.

Theorem 1: Consider the system given by (5) and (6) with $\boldsymbol{d} = \boldsymbol{0}_3$. If the control torque is set to $\boldsymbol{\tau}_{12} = \boldsymbol{\tau}_{12}^*$ with $k_1, k_2 > 0$, $0 < \alpha_1 < 1$ and $\alpha_2 = 2\alpha_1/(1+\alpha_1)$, then the closed-loop system is globally finite-time stable.

Proof: Since the global finite-time stability is a combination of global asymptotic stability and local finite-time stability. We intend to first show that the closed-loop system is globally asymptotically stable and then locally finite-time stable.

1) Global Asymptotic Stability: Choose a Lyapunov function candidate as follows:

$$V_1 = \frac{1}{2}\boldsymbol{\Omega}_{12}^T\boldsymbol{J}_{12}\boldsymbol{\Omega}_{12} + k_1\int_0^{\|\boldsymbol{w}\|}\frac{\phi^{\alpha_1}}{\sqrt{1+\phi^2}}\mathrm{d}\phi \tag{10}$$

where $V_1 = 0$ if and only if $\boldsymbol{\Omega}_{12} = \boldsymbol{0}_2$ and $\boldsymbol{w} = \boldsymbol{0}_2$.

The time derivative of V_1 is computed as

$$\dot{V}_1 = \boldsymbol{\Omega}_{12}^T\boldsymbol{J}_{12}\dot{\boldsymbol{\Omega}}_{12} + \frac{k_1}{\sqrt{1+\|\boldsymbol{w}\|^2}}\frac{\boldsymbol{w}^T\dot{\boldsymbol{w}}}{\|\boldsymbol{w}\|^{1-\alpha_1}}. \tag{11}$$

Note that the following equalities hold:

$$\begin{aligned}\boldsymbol{w}^T\boldsymbol{S}(\Omega_3)\boldsymbol{w} &= \boldsymbol{0}_2\\ \boldsymbol{w}^T\boldsymbol{F}(\boldsymbol{w}) &= \frac{1}{2}(1+\boldsymbol{w}^T\boldsymbol{w})\boldsymbol{w}^T\\ \boldsymbol{\Omega}_{12}^T\boldsymbol{J}_a\boldsymbol{S}(\Omega_3)\boldsymbol{\Omega}_{12} &= \boldsymbol{0}_2.\end{aligned}$$

Hence, substituting (5) and (9) into (11) yields

$$\dot{V}_1 = -k_2\boldsymbol{\Omega}_{12}^T\mathrm{sat}_{\alpha_2}(\boldsymbol{\Omega}_{12}) \leq 0 \tag{12}$$

which implies that the closed-loop system is Lyapunov stable, and $\lim_{t\to\infty} V_1(t)$ exists and is finite. Hence, $\boldsymbol{w}(t)$ and $\boldsymbol{\Omega}_{12}(t)$ are uniformly bounded. It then follows from (6) that $\dot{\boldsymbol{\Omega}}_{12}(t)$ is uniformly bounded and thus $\boldsymbol{\Omega}_{12}(t)$ is uniformly continuous. Recall the basic mathematical fact that a continuous function in a bounded space is uniformly continuous and the composition of two uniform continuous functions remains uniform continuous. It is then derived that $\dot{V}_1(t)$ is a uniform continuous function of t and Barablat's lemma [37] can be used to conclude that $\lim_{t\to\infty}\dot{V}_1(t) = 0$ and thus $\lim_{t\to\infty}\dot{\boldsymbol{\Omega}}_{12}(t) = \boldsymbol{0}_2$. Similar analyses can be used to show that $\dot{\boldsymbol{\Omega}}_{12}(t)$ is uniformly continuous as well. Once again, Barablat's lemma is applied to obtain $\lim_{t\to\infty}\boldsymbol{w}(t) = \boldsymbol{0}_2$. Therefore, the closed-loop system is globally asymptotically stable.

2) Local Finite-Time Stability: Since the system is globally asymptotically stable and our concern here is the local stability, it is reasonable to focus on the case that $(\boldsymbol{w}(t), \boldsymbol{\Omega}_{12}(t))$ stays in a neighborhood of the origin such that

$\text{sat}_{\alpha_2}(\boldsymbol{\Omega}_{12}) = \text{sgn}^{\alpha_2}(\boldsymbol{\Omega}_{12})$. Then, the system equations (5) and (9) are divided into a form similar to (2):

$$\begin{aligned}\dot{\boldsymbol{w}} &= \frac{1}{2}\boldsymbol{\Omega}_{12} + \hat{\boldsymbol{f}}_1(\boldsymbol{w}, \boldsymbol{\Omega}_{12}) \\ \dot{\boldsymbol{\Omega}}_{12} &= -k_1 \boldsymbol{J}_{12}^{-1} \frac{\boldsymbol{w}}{\|\boldsymbol{w}\|^{1-\alpha_1}} - k_2 \boldsymbol{J}_{12}^{-1} \text{sgn}^{\alpha_2}(\boldsymbol{\Omega}_{12}) \\ &\quad + \hat{\boldsymbol{f}}_2(\boldsymbol{w}, \boldsymbol{\Omega}_{12}) \end{aligned} \tag{13}$$

where $\hat{\boldsymbol{f}}_1(\boldsymbol{w}, \boldsymbol{\Omega}_{12})$ and $\hat{\boldsymbol{f}}_2(\boldsymbol{w}, \boldsymbol{\Omega}_{12})$ denote the higher-order terms and are given by

$$\begin{aligned}\hat{\boldsymbol{f}}_1(\boldsymbol{w}, \boldsymbol{\Omega}_{12}) &= \boldsymbol{S}(\Omega_3)\boldsymbol{w} + \frac{1}{2}(2\boldsymbol{w}\boldsymbol{w}^T - \boldsymbol{w}^T\boldsymbol{w}\boldsymbol{I}_2)\boldsymbol{\Omega}_{12} \\ \hat{\boldsymbol{f}}_2(\boldsymbol{w}, \boldsymbol{\Omega}_{12}) &= \boldsymbol{J}_{12}^{-1}\boldsymbol{J}_a\boldsymbol{S}(\Omega_3)\boldsymbol{\Omega}_{12} \\ &\quad - k_1 \boldsymbol{J}_{12}^{-1} \frac{\sqrt{1+\|\boldsymbol{w}\|^2}-1}{\sqrt{1+\|\boldsymbol{w}\|^2}} \frac{\boldsymbol{w}}{\|\boldsymbol{w}\|^{1-\alpha_1}}.\end{aligned}$$

Omitting $\hat{\boldsymbol{f}}_1(\boldsymbol{w}, \boldsymbol{\Omega}_{12})$ and $\hat{\boldsymbol{f}}_2(\boldsymbol{w}, \boldsymbol{\Omega}_{12})$, it can be shown by means of the same Lyapunov function candidate given in (10) that the low-order part of (13) is asymptotically stable. Construct a dilation Δ_λ^r such that $\Delta_\lambda^r(\boldsymbol{w}, \boldsymbol{\Omega}_{12}) = (\lambda^{r_1}\boldsymbol{w}, \lambda^{r_2}\boldsymbol{\Omega}_{12})$, where $r_1 = -2\,l/(1-\alpha_1)$, $r_2 = -(1+\alpha_1)l/(1-\alpha_1)$, and $l < 0$ is an arbitrary negative constant. Invoking $0 < \alpha_1 < 1$ and $\alpha_2 = 2\alpha_1/(1+\alpha_1)$, it is direct to verify that the low-order system is homogeneous of degree $l < 0$. Moreover, we can compute that

$$\begin{aligned}&\lim_{\lambda\to\infty} \frac{\hat{\boldsymbol{f}}_1(\lambda^{r_1}\boldsymbol{w}, \lambda^{r_2}\boldsymbol{\Omega}_{12})}{\lambda^{r_1+l}} \\ &= \lim_{\lambda\to\infty} \lambda^{-l}\boldsymbol{S}(\Omega_3)\boldsymbol{w} \\ &\quad + \lim_{\lambda\to\infty} 0.5\lambda^{r_1+r_2-l}(2\boldsymbol{w}\boldsymbol{w}^T - \boldsymbol{w}^T\boldsymbol{w}\boldsymbol{I}_2)\boldsymbol{\Omega}_{12} = \boldsymbol{0}_2 \\ &\lim_{\lambda\to\infty} \frac{\hat{\boldsymbol{f}}_2(\lambda^{r_1}\boldsymbol{w}, \lambda^{r_2}\boldsymbol{\Omega}_{12})}{\lambda^{r_1+l}} \\ &= \lim_{\lambda\to\infty} \lambda^{-l}\boldsymbol{J}_{12}^{-1}\boldsymbol{J}_a\boldsymbol{S}(\Omega_3)\boldsymbol{\Omega}_{12} \\ &\quad - \lim_{\lambda\to\infty} k_1 \boldsymbol{J}_{12}^{-1} \frac{\sqrt{1+\lambda^{2r_1}\|\boldsymbol{w}\|^2}-1}{\sqrt{1+\lambda^{2r_1}\|\boldsymbol{w}\|^2}} \frac{\boldsymbol{w}}{\|\boldsymbol{w}\|^{1-\alpha_1}} = \boldsymbol{0}_2.\end{aligned}$$

Therefore, Lemma 1 can be employed to assert that system (13) is locally finite-time stable. This together with the global asymptotic stability previously verified shows that the closed-loop system is globally finite-time stable. ■

Letting $\alpha_1 = 1$, (7) reduces to the saturated proportional-derivative controller designed in [27] for spin-axis stabilization. Furthermore, if we remove the scaling factor $1/\sqrt{1+\|\boldsymbol{w}\|^2}$ and the saturation function on $\boldsymbol{\Omega}_{12}$, we can obtain the proportional-derivative controller $\boldsymbol{\tau}_{12}^* = -k_1\boldsymbol{w} - k_2\boldsymbol{\Omega}_{12}$ derived in [22]. Therefore, controller (7) contains the control laws in [27] and [22] as special cases. Compared to [27] and [22], controller (7) ensures not only finite-time convergence but also bounded inputs. In addition, the fractional gain α_1 in (7) introduces more flexibility to tune the closed-loop performance.

B. ADAPTIVE ISM CONTROLLER WITH UNCERTAINTIES

Next, consider the case that the external disturbance is nonzero and Assumptions 2 and 3 hold. In addition, denote by $\boldsymbol{J}^* = \text{diag}\{J_1^*, J_2^*, J_3^*\}$ the known nominal values of the spacecraft inertia. Accordingly, the nominal values of $\boldsymbol{J}_{12}$ and $\boldsymbol{J}_a$ are given by

$$\boldsymbol{J}_{12}^* = \begin{bmatrix} J_1^* & 0 \\ 0 & J_2^* \end{bmatrix}, \quad \boldsymbol{J}_a^* = \boldsymbol{J}_{12}^* - J_3^*\boldsymbol{I}_2.$$

Inspired by the structural characteristic of the closed-loop dynamics given in (9), an integral sliding mode surface is designed as

$$\begin{aligned}\boldsymbol{s}(t) &= \boldsymbol{J}_{12}^*[\boldsymbol{\Omega}_{12}(t) - \boldsymbol{\Omega}_{12}(0)] \\ &\quad - \int_0^t [\boldsymbol{J}_a^*\boldsymbol{S}(\Omega_3(\phi))\boldsymbol{\Omega}_{12}(\phi) + \boldsymbol{\tau}_{12}^*(\phi)]\text{d}\phi.\end{aligned} \tag{14}$$

The above sliding mode relies on the nominal inertia of the spacecraft and the true inertia is not required. Since $\boldsymbol{s}(0) = 0$ for all initial conditions, the trajectory always starts from the sliding mode. This, however, does not mean that the closed-loop trajectory always stays on the sliding mode $\boldsymbol{s} = 0$ ever since the beginning time. The perturbations due to system uncertainties and measurement noise can drive the system trajectory away from the sliding mode. Later, adaptation techniques will be used to dynamically adjust the compensation for uncertainties according to the deviation from the sliding mode.

Once the system states are confined on the sliding mode since a certain moment, i.e., $\boldsymbol{s}(t) \equiv \boldsymbol{0}_2$, we have

$$\boldsymbol{J}_{12}^*[\boldsymbol{\Omega}_{12}(t) - \boldsymbol{\Omega}_{12}(0)] = \int_0^t [\boldsymbol{J}_a^*\boldsymbol{S}(\Omega_3(\phi))\boldsymbol{\Omega}_{12}(\phi) + \boldsymbol{\tau}^*(\phi)]\text{d}\phi$$

which is equivalent to

$$\begin{aligned}\boldsymbol{J}_{12}^*\dot{\boldsymbol{\Omega}}_{12} &= \boldsymbol{J}_a^*\boldsymbol{S}(\Omega_3)\boldsymbol{\Omega}_{12} \\ &\quad - \frac{k_1}{\sqrt{1+\|\boldsymbol{w}\|^2}} \frac{\boldsymbol{w}}{\|\boldsymbol{w}\|^{1-\alpha_1}} - k_2\text{sat}_{\alpha_2}(\boldsymbol{\Omega}_{12}).\end{aligned} \tag{15}$$

Evidently, the system dynamics on the sliding mode have a form similar to (9). The only difference is that the true inertia parameters are now replaced with their known nominal values. As a result, the stability results of Theorem 1 also hold for the system dynamics on the sliding mode. Thus, (14) gives a non-singular terminal sliding mode, as stated in the following lemma.

Lemma 2: Consider the integral sliding surface defined in (14) with $k_1, k_2 > 0$, $0 < \alpha_1 < 1$ and $\alpha_2 = 2\alpha_1/(1+\alpha_1)$. The system trajectory $(\boldsymbol{w}(t), \boldsymbol{\Omega}_{12}(t))$ globally converges to the origin in a finite time on the sliding mode $\boldsymbol{s}(t) \equiv \boldsymbol{0}_2$.

Differentiating (14) and substituting $\boldsymbol{\tau}_{12}^*$ with (7) leads to

$$\dot{\boldsymbol{s}} = \boldsymbol{J}_{12}^*\dot{\boldsymbol{\Omega}}_{12} - \boldsymbol{J}_a^*\boldsymbol{S}(\Omega_3)\boldsymbol{\Omega}_{12} - \boldsymbol{\tau}_{12}^*.$$

Employing (6) and letting

$$\Delta\boldsymbol{J}_{12} = \boldsymbol{J}_{12} - \boldsymbol{J}_{12}^* \quad \text{and } \Delta\boldsymbol{J}_a = \boldsymbol{J}_a - \boldsymbol{J}_a^*$$

we can derive via some algebraic manipulations that

$$\begin{aligned}\dot{\boldsymbol{s}} &= \boldsymbol{J}_{12}^*\boldsymbol{J}_{12}^{-1}[\boldsymbol{J}_a\boldsymbol{S}(\Omega_3)\boldsymbol{\Omega}_{12} + \boldsymbol{E}_{12}(t)\boldsymbol{\tau}_{12} + \boldsymbol{d}_{12}] \\ &\quad - \boldsymbol{J}_a^*\boldsymbol{S}(\Omega_3)\boldsymbol{\Omega}_{12} - \boldsymbol{\tau}_{12}^* \\ &= (\boldsymbol{I}_2 - \Delta\boldsymbol{J}_{12}\boldsymbol{J}_{12}^{-1})\boldsymbol{E}_{12}(t)(\boldsymbol{\tau}_{12} - \boldsymbol{\tau}_{12}^*) \\ &\quad - (\boldsymbol{I}_2 - \boldsymbol{E}_{12}(t))\boldsymbol{\tau}_{12}^* - \Delta\boldsymbol{J}_{12}\boldsymbol{J}_{12}^{-1}\boldsymbol{\tau}_{12}^*\end{aligned}$$

$$+\Delta\boldsymbol{J}_a\boldsymbol{S}(\Omega_3)\boldsymbol{\Omega}_{12}-\Delta\boldsymbol{J}_{12}\boldsymbol{J}_{12}^{-1}\boldsymbol{J}_a\boldsymbol{S}(\Omega_3)\boldsymbol{\Omega}_{12}$$
$$+(\boldsymbol{I}_2-\Delta\boldsymbol{J}_{12}\boldsymbol{J}_{12}^{-1})\boldsymbol{d}_{12}.$$

Rewritten this equation in a compact form as

$$\dot{\boldsymbol{s}}=(\boldsymbol{I}_2-\Delta\boldsymbol{J}_{12}\boldsymbol{J}_{12}^{-1})\boldsymbol{E}_{12}(t)(\boldsymbol{\tau}_{12}-\boldsymbol{\tau}_{12}^*)+\boldsymbol{p} \tag{16}$$

where $\boldsymbol{p}$ lumps the perturbing terms induced by actuator faults, unknown disturbance torques and inertia uncertainties, and is given by

$$\begin{aligned}\boldsymbol{p}=&-(\boldsymbol{I}_2-\boldsymbol{E}_{12}(t))\boldsymbol{\tau}_{12}^*-\Delta\boldsymbol{J}_{12}\boldsymbol{J}_{12}^{-1}\boldsymbol{\tau}_{12}^*\\&+\Delta\boldsymbol{J}_a\boldsymbol{S}(\Omega_3)\boldsymbol{\Omega}_{12}-\Delta\boldsymbol{J}_{12}\boldsymbol{J}_{12}^{-1}\boldsymbol{J}_a\boldsymbol{S}(\Omega_3)\boldsymbol{\Omega}_{12}\\&+(\boldsymbol{I}_2-\Delta\boldsymbol{J}_{12}\boldsymbol{J}_{12}^{-1})\boldsymbol{d}_{12}.\end{aligned}$$

Equation (8) and the Cauchy-Schwarz inequality can be used to show that

$$\begin{aligned}\|(\boldsymbol{I}_2-\boldsymbol{E}_{12}(t))\boldsymbol{\tau}_{12}^*\|&\le\chi_e(k_1+\sqrt{2}k_2)\\\|\Delta\boldsymbol{J}_{12}\boldsymbol{J}_{12}^{-1}\boldsymbol{\tau}_{12}^*\|&\le\|\Delta\boldsymbol{J}_{12}\boldsymbol{J}_{12}^{-1}\|(k_1+\sqrt{2}k_2)\end{aligned}$$

Similarly, we can further verify by invoking Assumptions 2 and 3 that

$$\begin{aligned}\|\Delta\boldsymbol{J}_a\boldsymbol{S}(\Omega_3)\boldsymbol{\Omega}_{12}\|&\le\delta_\omega\|\Delta\boldsymbol{J}_a\|\|\boldsymbol{\Omega}_{12}\|\\\|\Delta\boldsymbol{J}_{12}\boldsymbol{J}_{12}^{-1}\boldsymbol{J}_a\boldsymbol{S}(\Omega_3)\boldsymbol{\Omega}_{12}\|&\le\delta_\omega\|\Delta\boldsymbol{J}_{12}\boldsymbol{J}_{12}^{-1}\boldsymbol{J}_a\|\|\boldsymbol{\Omega}_{12}\|\\\|(\boldsymbol{I}_2-\Delta\boldsymbol{J}_{12}\boldsymbol{J}_{12}^{-1})\boldsymbol{d}_{12}\|&\le\delta_d\|\boldsymbol{I}_2-\Delta\boldsymbol{J}_{12}\boldsymbol{J}_{12}^{-1}\|.\end{aligned}$$

Summarizing the above bounds, one can obtain

$$\|\boldsymbol{p}\|\le\eta(1+\|\boldsymbol{\Omega}_{12}\|) \tag{17}$$

where

$$\begin{aligned}\eta=\max\Big\{&(\chi_e+\|\Delta\boldsymbol{J}_{12}\boldsymbol{J}_{12}^{-1}\|)(k_1+\sqrt{2}k_2)\\&+\delta_d\|\boldsymbol{I}_2-\Delta\boldsymbol{J}_{12}\boldsymbol{J}_{12}^{-1}\|,\delta_\omega\|\Delta\boldsymbol{J}_a\|+\delta_\omega\|\Delta\boldsymbol{J}_{12}\boldsymbol{J}_{12}^{-1}\boldsymbol{J}_a\|\Big\}.\end{aligned}$$

Since the inertias $\Delta\boldsymbol{J}_{12}$, $\boldsymbol{J}_{12}$, $\Delta\boldsymbol{J}_a$, and $\boldsymbol{J}_a$ are all constants as stated in Assumption 1, it follows that $\eta>0$ is a constant. Due to the presence of uncertainties, η is unknown. An adaptively tuned variable $\hat{\eta}$ is introduced as an estimate of η in order to compensate for the lumped unknown perturbations. A novel adaptive controller based on the ISM given in (14) is then designed as

$$\boldsymbol{\tau}_{12}=\boldsymbol{\tau}_{12}^*-k_3\boldsymbol{s}-\hat{\eta}(1+\|\boldsymbol{\Omega}_{12}\|)\boldsymbol{s}_a \tag{18}$$

where $k_3>0$ and

$$\boldsymbol{s}_a=\begin{cases}\dfrac{\boldsymbol{s}}{\|\boldsymbol{s}\|} & \text{if } \hat{\eta}(1+\|\boldsymbol{\Omega}_{12}\|)\|\boldsymbol{s}\|>\epsilon\\[2ex]\dfrac{\hat{\eta}(1+\|\boldsymbol{\Omega}_{12}\|)\boldsymbol{s}}{\epsilon} & \text{if } \hat{\eta}(1+\|\boldsymbol{\Omega}_{12}\|)\|\boldsymbol{s}\|\le\epsilon\end{cases} \tag{19}$$

where $\epsilon>0$ is a constant. The adaptive variable $\hat{\eta}$ is updated by the following equation

$$\dot{\hat{\eta}}=-\rho_1\hat{\eta}+\rho_2(1+\|\boldsymbol{\Omega}_{12}\|)\|\boldsymbol{s}\|,\quad\hat{\eta}(0)\ge0 \tag{20}$$

where $\rho_1,\rho_2>0$.

The control torque given in (18) consists of three parts. The nominal part $\boldsymbol{\tau}_{12}^*$ denotes the torques required on the sliding mode and the linear part $-k_3\boldsymbol{s}$ provides torques pulling the system trajectory to the sliding mode. In particular, the adaptive part $-\hat{\eta}(1+\|\boldsymbol{\Omega}_{12}\|)\boldsymbol{s}_a$ aims to compensate for the perturbations. When $\boldsymbol{s}$ is stabilized to the vicinity of zero, the performance of controller (7) is approximately recovered.

The above observation enables us to obtain some rules on parameter tuning. Increasing k_1 and k_2 enlarges the spring force and damping effect of the sliding mode dynamics, respectively. Increasing k_3 amplifies the stabilizing effect to the ISM surface and meanwhile the magnitude of required control torques. ρ_1 and ρ_2 determine the sensitivity of the updating law on state errors. Increasing ρ_2 enables to adjust the parameter estimate $\hat{\eta}$ quickly when state errors are large. In contrast, increasing ρ_1 enforces the damping in the updating law and can avoid excessive growth of the parameter estimate. With the boundary layer given in (19), the control torque is continuous and the chattering effect can be mitigated by properly selecting the parameter ϵ. Generally, decreasing the values of ϵ can reduce the ultimate state errors but increase the risk of inducing chattering effect in control torques.

The proposed adaptive ISM controller incorporates a finite-time convergent sliding mode dynamics and an adaptive algorithm to estimate and compensate for the perturbations. Hence, it has better robustness against uncertain inertia, unknown disturbances, and actuator faults than the existing methods derived in [22], [23], [25]–[27]. Note that these methods did not take actuator faults into consideration. In addition, the proposed controller has a clear physical meaning and thus its gain tuning is greatly simplified.

The stability of the entire closed-loop system is summarized in the following theorem.

Theorem 2: Consider the system given in (5) and (6), and the adaptive controller given in (18)-(20). The control parameters satisfy $k_1,k_2,k_3>0$, $0<\alpha_1<1$, $\alpha_2=2\alpha_1/(1+\alpha_1)$, and $\rho_1,\rho_2>0$. Then, all the closed-loop states are uniformly bounded and $(\boldsymbol{w}(t),\boldsymbol{\Omega}_{12}(t))$ is stabilized to the following neighborhood of $\boldsymbol{s}(t)=\boldsymbol{0}_2$:

$$\|\boldsymbol{s}\|<\sqrt{\frac{2\rho_1\eta^2+\chi^2\rho_2\epsilon}{2\chi\rho_2\min\{2\chi k_3,\rho_1\}}} \tag{21}$$

where $\chi=1-\chi_e-\|\Delta\boldsymbol{J}_{12}\boldsymbol{J}_{12}^{-1}\|$.

Proof: First, note that $\chi>0$ according to Assumption (4). Choose a Lyapunov function candidate as

$$V_2=\frac{1}{2}\boldsymbol{s}^T\boldsymbol{s}+\frac{1}{2\chi\rho_2}(\eta-\chi\hat{\eta})^2. \tag{22}$$

Clearly, V_2 satisfies $V_2\ge0$ and $V_2=0$ if and only if $\boldsymbol{s}=\boldsymbol{0}_2$ and $\eta=\chi\hat{\eta}$.

Differentiating V_2 along (16) and invoking (17) produces

$$\begin{aligned}\dot{V}_2&=\boldsymbol{s}^T\dot{\boldsymbol{s}}-\frac{1}{\rho_2}(\eta-\chi\hat{\eta})\dot{\hat{\eta}}\\&=\boldsymbol{s}^T(\boldsymbol{I}_2-\Delta\boldsymbol{J}_{12}\boldsymbol{J}_{12}^{-1})\boldsymbol{E}_{12}(t)(\boldsymbol{\tau}_{12}-\boldsymbol{\tau}_{12}^*)\\&\quad+\boldsymbol{s}^T\boldsymbol{p}-\frac{1}{\rho_2}(\eta-\chi\hat{\eta})\dot{\hat{\eta}}\end{aligned}$$

$$\begin{aligned}
&\leq \boldsymbol{s}^T(\boldsymbol{I}_2 - \Delta\boldsymbol{J}_{12}\boldsymbol{J}_{12}^{-1})\boldsymbol{E}_{12}(t)(\boldsymbol{\tau}_{12} - \boldsymbol{\tau}_{12}^*) \\
&\quad + \eta(1 + \|\boldsymbol{\Omega}_{12}\|)\|\boldsymbol{s}\| - \frac{1}{\rho_2}(\eta - \chi\hat{\eta})\dot{\hat{\eta}} \\
&= N_s + \chi\hat{\eta}(1 + \|\boldsymbol{\Omega}_{12}\|)\|\boldsymbol{s}\| \\
&\quad - \frac{1}{\rho_2}(\eta - \chi\hat{\eta})(\dot{\hat{\eta}} - \rho_2(1 + \|\boldsymbol{\Omega}_{12}\|)\|\boldsymbol{s}\|) \qquad (23)
\end{aligned}$$

where

$$\begin{aligned}
N_s &= \boldsymbol{s}^T(\boldsymbol{I}_2 - \Delta\boldsymbol{J}_{12}\boldsymbol{J}_{12}^{-1})\boldsymbol{E}_{12}(t)(\boldsymbol{\tau}_{12} - \boldsymbol{\tau}_{12}^*) \\
&= \boldsymbol{s}^T(\boldsymbol{\tau}_{12} - \boldsymbol{\tau}_{12}^*) - \boldsymbol{s}^T(\boldsymbol{I}_2 - \boldsymbol{E}_{12}(t))(\boldsymbol{\tau}_{12} - \boldsymbol{\tau}_{12}^*) \\
&\quad - \boldsymbol{s}^T\Delta\boldsymbol{J}_{12}\boldsymbol{J}_{12}^{-1}(\boldsymbol{\tau}_{12} - \boldsymbol{\tau}_{12}^*). \qquad (24)
\end{aligned}$$

Recalling $\|\boldsymbol{s}^T(\boldsymbol{I}_2 - \boldsymbol{E}_{12}(t))(\boldsymbol{\tau}_{12} - \boldsymbol{\tau}_{12}^*)\| \leq \chi_e\|\boldsymbol{s}\|\|\boldsymbol{\tau}_{12} - \boldsymbol{\tau}_{12}^*\|$ and $\|\Delta\boldsymbol{J}_{12}\boldsymbol{J}_{12}^{-1}(\boldsymbol{\tau}_{12} - \boldsymbol{\tau}_{12}^*)\| \leq \|\Delta\boldsymbol{J}_{12}\boldsymbol{J}_{12}^{-1}\|\|\boldsymbol{s}\|\|\boldsymbol{\tau}_{12} - \boldsymbol{\tau}_{12}^*\|$, and substituting $\boldsymbol{\tau}_{12}$ with (18) into (24) yields

$$\begin{aligned}
N_s \leq\ & -k_3\|\boldsymbol{s}\|^2 - \hat{\eta}(1 + \|\boldsymbol{\Omega}_{12}\|)\|\boldsymbol{s}\|\|\boldsymbol{s}_a\| \\
& + \chi_e k_3\|\boldsymbol{s}\|^2 + \chi_e\hat{\eta}(1 + \|\boldsymbol{\Omega}_{12}\|)\|\boldsymbol{s}\|\|\boldsymbol{s}_a\| \\
& + k_3\|\Delta\boldsymbol{J}_{12}\boldsymbol{J}_{12}^{-1}\|\|\boldsymbol{s}\|^2 \\
& + \|\Delta\boldsymbol{J}_{12}\boldsymbol{J}_{12}^{-1}\|\hat{\eta}(1 + \|\boldsymbol{\Omega}_{12}\|)\|\boldsymbol{s}\|\|\boldsymbol{s}_a\| \qquad (25)
\end{aligned}$$

where the property $\boldsymbol{s}^T\boldsymbol{s}_a = \|\boldsymbol{s}^T\|\|\boldsymbol{s}_a\|$ is utilized in deriving (25).

Substituting $\dot{\hat{\eta}}$ with (20) and (25) into (23) and invoking $\chi = 1 - \chi_e - \|\Delta\boldsymbol{J}_{12}\boldsymbol{J}_{12}^{-1}\|$ yields

$$\begin{aligned}
\dot{V}_2 \leq\ & -\chi_e k_3\|\boldsymbol{s}\|^2 - \chi_e\hat{\eta}(1 + \|\boldsymbol{\Omega}_{12}\|)\|\boldsymbol{s}\|\|\boldsymbol{s}_a\| \\
& + \chi\hat{\eta}(1 + \|\boldsymbol{\Omega}_{12}\|)\|\boldsymbol{s}\| - \frac{\rho_1}{\rho_2}(\eta - \chi\hat{\eta})\hat{\eta}. \qquad (26)
\end{aligned}$$

In addition, it is direct to verify that

$$\begin{aligned}
(\eta - \chi\hat{\eta})(\chi\hat{\eta}) &= -(\eta - \chi\hat{\eta})(\eta - \chi\hat{\eta} - \eta) \\
&\leq -\frac{(\eta - \chi\hat{\eta})^2}{2} + \frac{\eta^2}{2}.
\end{aligned}$$

Consequently, (26) further leads to

$$\begin{aligned}
\dot{V}_2 &\leq -\chi k_3\|\boldsymbol{s}\|^2 - \chi\hat{\eta}(1 + \|\boldsymbol{\Omega}_{12}\|)\|\boldsymbol{s}\|\|\boldsymbol{s}_a\| \\
&\quad + \chi\hat{\eta}(1 + \|\boldsymbol{\Omega}_{12}\|)\|\boldsymbol{s}\| - \frac{\rho_1}{2\chi\rho_2}(\eta - \chi\hat{\eta})^2 + \frac{\rho_1\eta^2}{2\chi\rho_2} \\
&= -\chi k_3\|\boldsymbol{s}\|^2 + \chi\hat{\eta}(1 + \|\boldsymbol{\Omega}_{12}\|)\|\boldsymbol{s}\|(1 - \|\boldsymbol{s}_a\|) \\
&\quad - \frac{\rho_1}{2\chi\rho_2}(\eta - \chi\hat{\eta})^2 + \frac{\rho_1\eta^2}{2\chi\rho_2}. \qquad (27)
\end{aligned}$$

Recalling the expression of $\boldsymbol{s}_a$ given in (19), it can be seen that $\chi\hat{\eta}(1+\|\boldsymbol{\Omega}_{12}\|)\|\boldsymbol{s}\|(1-\|\boldsymbol{s}_a\|) = 0$ when $\hat{\eta}(1+\|\boldsymbol{\Omega}_{12}\|)\|\boldsymbol{s}\| > \epsilon$. When $\hat{\eta}(1 + \|\boldsymbol{\Omega}_{12}\|)\|\boldsymbol{s}\| \leq \epsilon$, the following inequality can be verified:

$$\begin{aligned}
&\chi\hat{\eta}(1 + \|\boldsymbol{\Omega}_{12}\|)\|\boldsymbol{s}\|(1 - \|\boldsymbol{s}_a\|) \\
&\quad = \frac{\chi}{\epsilon}\hat{\eta}(1 + \|\boldsymbol{\Omega}_{12}\|)\|\boldsymbol{s}\|(\epsilon - \hat{\eta}(1 + \|\boldsymbol{\Omega}_{12}\|)\|\boldsymbol{s}\|) \\
&\quad \leq \frac{\chi\epsilon}{4}.
\end{aligned}$$

Letting

$$\gamma_0 = \frac{\rho_1\eta^2}{2\chi\rho_2} + \frac{\chi\epsilon}{4}$$

we can then deduce from (27) that

$$\begin{aligned}
\dot{V}_2 &\leq -\chi k_3\|\boldsymbol{s}\|^2 - \frac{\rho_1}{2\chi\rho_2}(\eta - \chi\hat{\eta})^2 + \gamma_0 \\
&\leq -\gamma_1 V_2 + \gamma_0 \qquad (28)
\end{aligned}$$

where $\gamma_1 = \min\{2\chi k_3, \rho_1\} > 0$ according to Assumption 4. It can then be concluded by means of Theorem 4.18 in [37] that the states of the closed-loop system are all uniformly bounded and ultimately stabilized to the following region

$$V_2 < \frac{\gamma_0}{\gamma_1} = \frac{2\rho_1\eta^2 + \chi^2\rho_2\epsilon}{4\chi\rho_2\min\{2\chi k_3, \rho_1\}}.$$

Noting that $\|\boldsymbol{s}\| \leq \sqrt{2V_2}$, we can finally deduce that the sliding function is stabilized to the region given by (21). The conclusion in Theorem 2 is now obtained. ■

IV. NUMERICAL EXAMPLES

In this section, numerical simulations are performed to the demonstrate the efficacy of the proposed methods. The first example compares the performance of the Hölder-continuous controller given by (7) and the adaptive controller given by (18)-(20). More precisely, the Hölder-continuous controller is simulated in the absence of uncertainties while the adaptive ISM controller is simulated in the presence of multiple uncertainties. The second example compares the performance of the proposed adaptive ISM controller with three existing spin-axis stabilization controllers, namely, the optimal controller derived in [23], the internal-model-based controller derived in [25] and the adaptive sliding mode controller designed in [27].

Consider a nearly axis-symmetric spacecraft with $\hat{\boldsymbol{b}}_3$-axis being the symmetry axis. The symmetry axis is unactuated and there are two control torques along $\hat{\boldsymbol{b}}_1$ and $\hat{\boldsymbol{b}}_2$, which are perpendicular to $\hat{\boldsymbol{b}}_3$-axis. The torque saturation limit is 2 N·m. The true inertia matrix of the spacecraft is

$$\boldsymbol{J} = \begin{bmatrix} 30 & 3 & -1 \\ 3 & 28 & -2 \\ -1 & -2 & 60 \end{bmatrix} \text{ kg} \cdot \text{m}^2.$$

while the nominal inertia used for control is assumed to be $\boldsymbol{J}^* = \text{diag}\{32, 32, 65\}$ kg · m^2. Additionally, the external disturbance acting on the spacecraft is given by

$$\boldsymbol{d}(t) = \begin{bmatrix} 0.1 + 0.5\cos(0.15t) \\ -0.2 + 0.6\cos(0.15t) \\ 0.04\cos(0.075t) + 0.04\sin(0.15t) \end{bmatrix} \text{N} \cdot \text{m}.$$

The 1st and 2nd actuators are assumed to encounter fault profiles of $e_1(t) = 0.7 + 0.1\sin(0.1\ t)$ and $e_2(t) = 0.8 - 0.1\cos(0.1\ t)$, respectively. The desired inertial direction is $[0, 0, 1]^T$. The influence of measurement noise is considered in the simulations. The measured attitude and angular velocity used for control law implementation are assumed to be $\boldsymbol{w}_m = \boldsymbol{w} + \boldsymbol{n}_w$ and $\boldsymbol{\Omega}_m = \boldsymbol{\Omega} + \boldsymbol{n}_\Omega$, where $\boldsymbol{n}_w$ and $\boldsymbol{n}_\Omega$ are white Gaussian noise processes subject to the distributions $\mathcal{N}(\boldsymbol{0}_2, (1 \times 10^{-4})^2\boldsymbol{I}_2)$ and $\mathcal{N}(\boldsymbol{0}_2, (1 \times 10^{-6}\ \text{rad/s})^2\boldsymbol{I}_2)$, respectively.

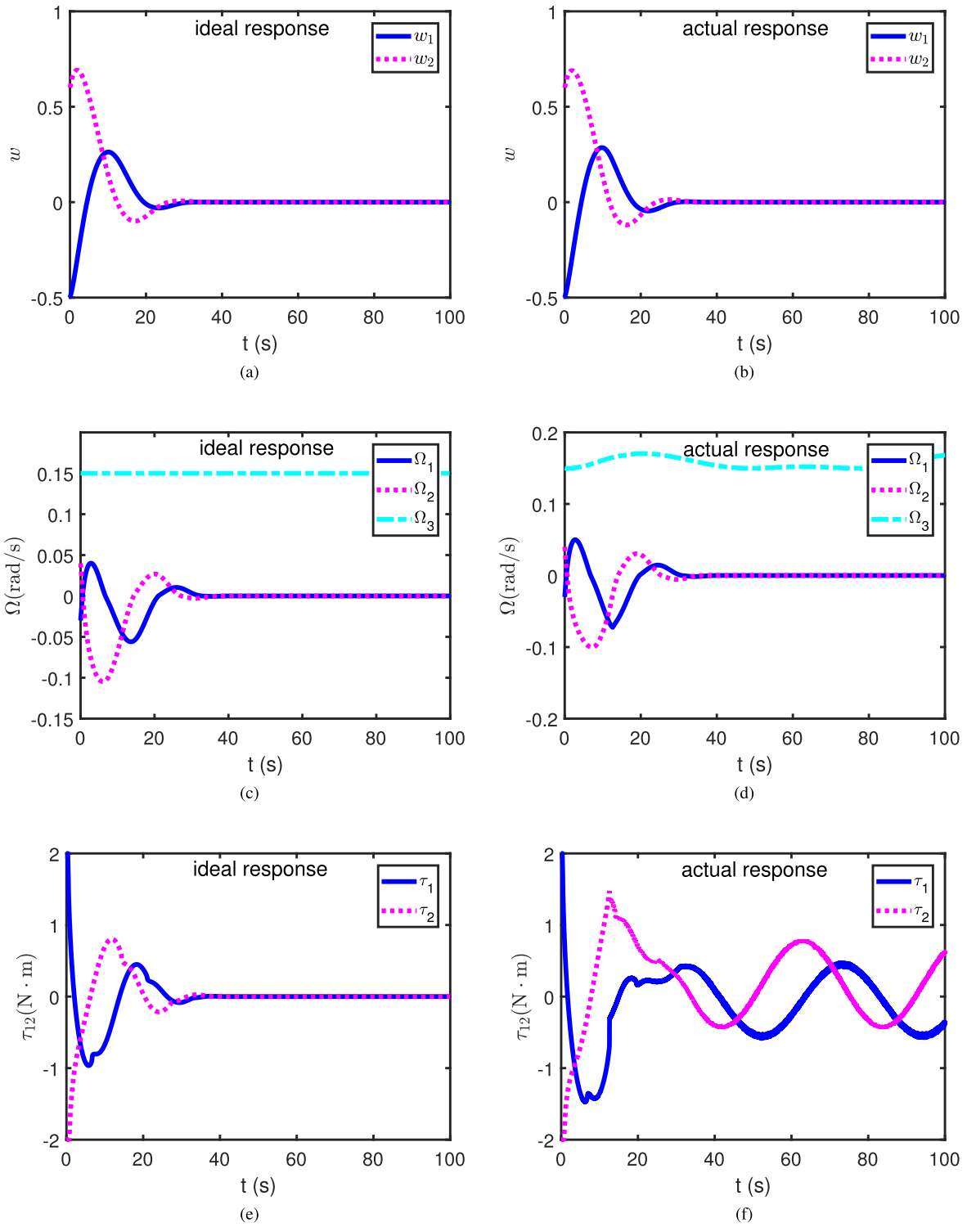

FIGURE 2. Comparison of the ideal and actual performance for the adaptive ISM controller given by (18)-(20): (a, b) w coordinate, (c, d) angular velocity, and (e, f) command torque.

A. COMPARISON WITH CONTROLLER (7)

Assume that the initial conditions of the spacecraft are $\boldsymbol{w}(0) = [-0.5, 0.6]^T$, $z(0) = -0.4$, and $\boldsymbol{\Omega}(0) = [-0.03, 0.04, 0.15]^T$ rad/s. First, the Hölder-continuous controller is simulated with no uncertainties, i.e., $\boldsymbol{J} = \boldsymbol{J}^* = \text{diag}\{32, 32, 65\}$ kg · m^2, $\boldsymbol{d} = \boldsymbol{0}_3$, and $\boldsymbol{E}_{12}(t) = \boldsymbol{I}_2$. Following this, the adaptive ISM controller is simulated by considering the inertia uncertainties, external disturbances, and actuator faults specified

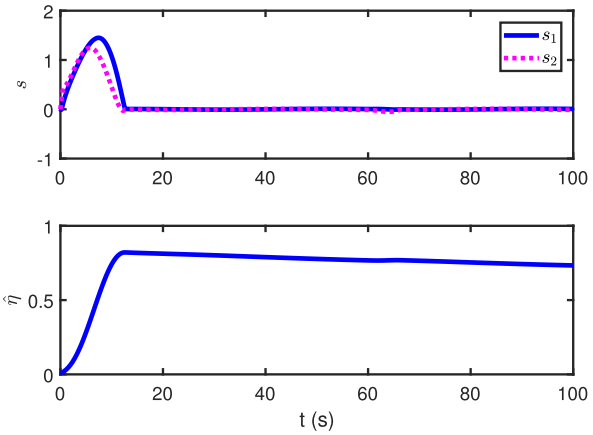

FIGURE 3. Responses of the sliding function s and adaptive variable $\hat{\eta}$ for the adaptive ISM controller given by (18)-(20) under multiple system uncertainties.

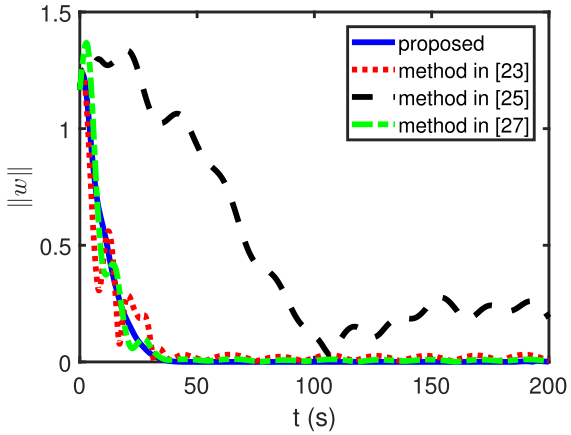

FIGURE 4. Time histories of $\|\boldsymbol{w}\|$.

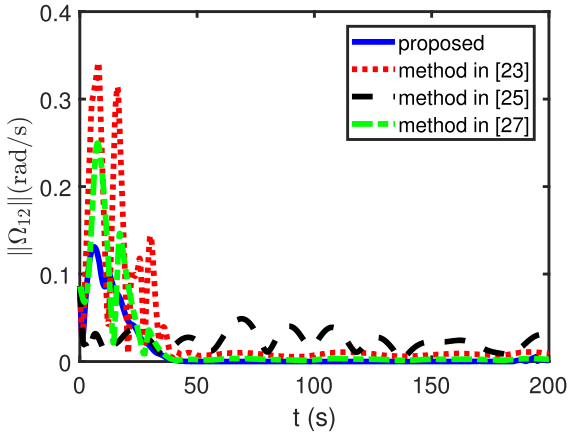

FIGURE 5. Time histories of $\|\boldsymbol{\Omega}_{12}\|$.

previously. The control gains for controller (7) are set to $k_1 = 4$, $k_2 = 12$, $\alpha_1 = 0.6$ and $\alpha_2 = 0.75$. For the adaptive controller, we set $k_3 = 0.01$, $\rho_1 = 0.002$, $\rho_2 = 0.05$, $\epsilon = 0.01$ $\hat{\eta}(0) = 0.01$ and maintain k_1, k_2, α_1 and α_2 the same as controller (7).

Fig. 2 compares the resultant responses of $\boldsymbol{w}$ coordinate, angular velocity Ω, and command torque $\boldsymbol{\tau}_{12}$ by controller (7) and the adaptive ISM controller. When there are no uncertainties, controller (7) yields closed-loop dynamics given by (9), which is equivalent to the ideal sliding dynamics on the ISM $\boldsymbol{s} = \boldsymbol{0}_2$, i.e., (15). Therefore, the first simulation and its results given in Figs. 2a, 2c, and 2e correspond to the ideal performance of the adaptive ISM controller when $\boldsymbol{s} = \boldsymbol{0}_2$ is maintained precisely from the beginning to the end of the simulation. In this case, the symmetry axis is stabilized to the desired direction in about 40 seconds. Figs. 2b, 2d, and 2f plot the actual responses of $\boldsymbol{w}$, $\boldsymbol{\Omega}$, and $\boldsymbol{\tau}_{12}$ of the adaptive ISM controller under multiple system uncertainties. Fig. 3 plots the time histories of the sliding variable $\boldsymbol{s}$ and adaptive parameter $\hat{\eta}$. Despite the influence of multiple system uncertainties, the actual performance of $\boldsymbol{w}$ and $\boldsymbol{\Omega}$ has very minor difference with the ideal performance. The reason can be found from Fig. 3. The initial angular velocity and system uncertainties bring the attitude trajectory away from the sliding mode $\boldsymbol{s} = \boldsymbol{0}_2$. This triggers the adaptive algorithm to increase $\hat{\eta}$ so that the attitude trajectory is pulled back to the vicinity of $\boldsymbol{s} = \boldsymbol{0}_2$ after 15 seconds. In order to reject the influence of system uncertainties, the resultant command torque is nonzero and time-varying in the steady phase (Fig. 2f) as opposed to the ideal case (Fig. 2e), which is zero in the steady phase. Therefore, the adaptive ISM controller can quickly and efficiently compensate for the system uncertainties and approximately recover the ideal performance specified by the ISM dynamics.

B. COMPARISON WITH EXISTING METHODS

The simulations in this subsection compares the performance of the proposed adaptive ISM controller with the spin-axis stabilizing control laws derived in [23], [25], [27] in the presence of system uncertainties described in the preceding. The initial conditions of the spacecraft are renewed to $\boldsymbol{w}(0) = [1, -0.6]^T$, $z(0) = -1$, and $\boldsymbol{\Omega}(0) = [0.05, -0.07, 0.15]^T$ rad/s. The torque saturation limit and control parameters for the adaptive ISM controller remain the same as the previous simulation. The gains for the methods in [23], [25], [27] are tuned such that the convergence time for $\|\boldsymbol{w}\|$ and $\boldsymbol{\Omega}$ is as close to that by the adaptive ISM controller as possible. The resultant gains are $k = 0.1$ and $\lambda = 0.8$ for the method in [23], $k = 15$ and $\sigma = 20$ for the method in [25], and $k_1 = 0.5$, $\rho_1 = \rho_2 = 0.5$, $r_1 = r_2 = 0.1$, $\alpha = 0.8$, $\epsilon = 0.001$, $p_1 = 0.3$, $p_2 = 0.2$, and $\theta_1(0) = \theta_2(0) = 0.01$ for the method in [27].

The simulation results are given in Figs. 4-6, which compare the time histories of $\|\boldsymbol{w}\|$, $\|\boldsymbol{\Omega}_{12}\|$, and $\boldsymbol{\tau}_{12}$ by the four methods. The proposed method and the methods in [23], [27] attain a convergence time of about 40 seconds for $\|\boldsymbol{w}\|$ and $\|\boldsymbol{\Omega}_{12}\|$. The method in [25] yields the longest convergence time. We can also see that the proposed method achieves much smoother transient responses than the other three methods.

Table 1 summarizes and compares the steady-state accuracy attained by the four control methods. The residual errors

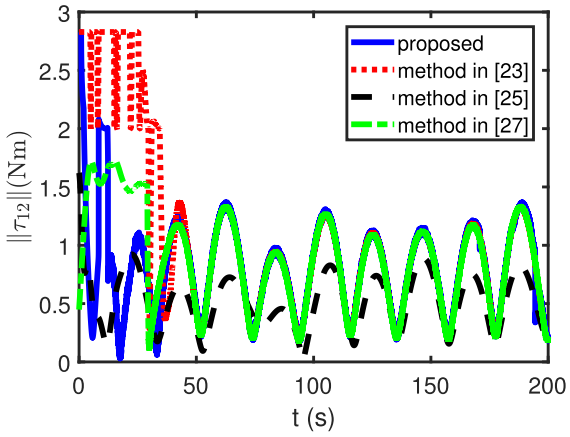

FIGURE 6. Time histories of $\|\tau_{12}\|$.

TABLE 1. Comparison of the steady-state pointing accuracy.

methods	$\|\boldsymbol{w}\|$	$\|\boldsymbol{\Omega}_{12}\|$ (rad/s)
proposed	1.08×10^{-5}	2.31×10^{-5}
controller in [23]	2.94×10^{-2}	1.07×10^{-2}
controller in [25]	0.26	3.9×10^{-2}
controller in [27]	1.08×10^{-2}	3.4×10^{-3}

of $\|\boldsymbol{w}\|$ and $\|\boldsymbol{\Omega}_{12}\|$ for the proposed method are 1.08×10^{-5} and 2.31×10^{-5} rad/s, respectively, which are far smaller than those for the other three methods. Note that the methods in [23], [25] exhibit poor robustness because they rely on precise inertia matrix, fully healthy actuators, and satisfactory disturbance compensation. The sliding mode controller in [27] utilizes adaptive techniques to reject disturbances but the sliding mode motion ensures merely asymptotic convergence. In summary, the proposed method has better robustness against inertia uncertainties, external disturbances, and actuator faults. This advantage is due to the finite-time convergent sliding mode dynamics and the adaptive mechanism for perturbation compensation. As a result, the proposed adaptive ISM controller ensures better transient responses and higher steady-state accuracy.

V. CONCLUSION

Two controllers were proposed to stabilize the spinning axis of an axis-symmetric spacecraft to any desired inertial direction using two torques normal to the symmetry axis. The first is a non-smooth yet continuous controller with a nonlinear proportional-derivative structure, which was developed via the homogeneous theory without any uncertainties. It was further utilized to construct an integral sliding mode surface, based on which a novel adaptive controller was developed to deal with uncertain inertia, unknown disturbances and actuator faults. The adaptive controller can approximately recover the performance of the non-smooth controller to achieve high pointing accuracy of the spacecraft spinning axis, even in the presence of multiple uncertainties. The effectiveness of the proposed methods was demonstrated by numerical examples.

REFERENCES

[1] N. Dennehy, "Spacecraft hybird control at nasa: A historical look back, current initiatives, and some future consideratons," in *Proc. 37th Annu. AAS Guid. Control Conf.*, Breckenridge, CO, USA: AAS, 2014, pp. 1–21.
[2] C. D. Petersen, F. Leve, M. Flynn, and I. Kolmanovsky, "Recovering linear controllability of an underactuated spacecraft by exploiting solar radiation pressure," *J. Guid., Control, Dyn.*, vol. 39, no. 4, pp. 826–837, Apr. 2016.
[3] A. Frias, "Nonlinear attitude control of underactuated spacecraft," Ph.D. dissertation, Dept. Aerosp. Eng., Ryerson Univ., Toronto, ON, Canada, vol. 109, 2019.
[4] A. Zavoli, G. De Matteis, F. Giulietti, and G. Avanzini, "Single-axis pointing of an underactuated spacecraft equipped with two reaction wheels," *J. Guid., Control, Dyn.*, vol. 40, no. 6, pp. 1465–1471, Jun. 2017.
[5] H. Kojima, K. Hiraiwa, and Y. Yoshimura, "Experimental study on line-of-sight (LOS) attitude control using control moment gyros under micro-gravity environment," *Acta Astronautica*, vol. 143, pp. 118–125, Feb. 2018.
[6] H. Gui and G. Vukovich, "Attitude stabilization of a spacecraft with two parallel control moment gyros," *AIAA J. Guid., Control, Dyn.*, vol. 39, no. 3, pp. 728–735, 2016.
[7] C. D. Petersen, F. Leve, and I. Kolmanovsky, "Underactuated spacecraft switching law for two reaction wheels and constant angular momentum," *J. Guid., Control, Dyn.*, vol. 39, no. 9, pp. 2086–2099, Sep. 2016.
[8] T. Fukaishi, K. Sekiguchi, and K. Nonaka, "Attitude control of two-wheel spacecraft based on dynamics model via hierarchical linearization," *SICE J. Control, Meas., Syst. Integr.*, vol. 10, no. 4, pp. 310–316, 2017.
[9] J. D. Biggs, Y. Bai, and H. Henninger, "Attitude guidance and tracking for spacecraft with two reaction wheels," *Int. J. Control*, vol. 91, no. 4, pp. 926–936, Apr. 2018.
[10] C. Yue, K. D. Kumar, Q. Shen, C. H. Goh, and T. H. Lee, "Attitude stabilization using two parallel single-gimbal control moment gyroscopes," *J. Guid., Control, Dyn.*, vol. 42, no. 6, pp. 1353–1364, Jun. 2019.
[11] A. Golzari, H. N. Pishkenari, H. Salarieh, and T. Abdollahi, "Quaternion based linear time-varying model predictive attitude control for satellites with two reaction wheels," *Aerosp. Sci. Technol.*, vol. 98, no. 105677, pp. 1–10, 2020.
[12] H. Gui, G. Vukovich, and S. Xu, "Attitude tracking of a rigid spacecraft using two internal torques," *IEEE Trans. Aerosp. Electron. Syst.*, vol. 51, no. 4, pp. 2900–2913, Oct. 2015.
[13] P. Morin and C. Samson, "Time-varying exponential stabilization of a rigid spacecraft with two control torques," *IEEE Trans. Autom. Control*, vol. 42, no. 4, pp. 528–534, Apr. 1997.
[14] P. Tsiotras and J. Luo, "Control of underactuated spacecraft with bounded inputs," *Automatica*, vol. 36, no. 8, pp. 1153–1169, Aug. 2000.
[15] D. Casagrande, A. Astolfi, and T. Parisini, "Global asymptotic stabilization of the attitude and the angular rates of an underactuated non-symmetric rigid body," *Automatica*, vol. 44, no. 7, pp. 1781–1789, Jul. 2008.
[16] M. Mirshams and M. Khosrojerdi, "Attitude control of an underactuated spacecraft using tube-based MPC approach," *Aerosp. Sci. Technol.*, vol. 48, pp. 140–145, Jan. 2016.
[17] A.-M. Zou, K. Dev Kumar, and A. H. J. de Ruiter, "Spacecraft attitude control using two control torques," *Inf. Sci.*, vol. 408, pp. 23–40, Oct. 2017.
[18] A. Frias, A. H. J. de Ruiter, and K. D. Kumar, "Velocity-free attitude stabilization of a nadir-pointing underactuated rigid spacecraft," *J. Guid., Control, Dyn.*, vol. 41, no. 5, pp. 1068–1082, May 2018.
[19] A. Frias, A. H. J. de Ruiter, and K. D. Kumar, "Velocity-free spacecraft attitude stabilization using two control torques," *Automatica*, vol. 109, no. 108553, pp. 1–8, 2019.
[20] P. E. Crouch, "Spacecraft attitude control and stabilization: Application of geometric control theory to rigid body models," *IEEE Trans. Autom. Control*, vol. 29, no. 4, pp. 321–331, Apr. 1984.
[21] H. Krishnan, M. Reyhanoglu, and H. McClamroch, "Attitude stabilization of a rigid spacecraft using two control torques: A nonlinear control approach based on the spacecraft attitude dynamics," *Automatica*, vol. 30, no. 6, pp. 1023–1027, Jun. 1994.
[22] P. Tsiotras and J. M. Longuski, "Spin-axis stabilization of symmetric spacecraft with two control torques," *Syst. Control Lett.*, vol. 23, no. 6, pp. 395–402, Dec. 1994.
[23] P. Tsiotras, "Optimal regulation and passivity results for axisymmetric rigid bodies using two controls," *AIAA J. Guid., Control, Dyn.*, vol. 20, no. 3, pp. 457–464, 1997.
[24] Y. Cheon, "Spin-axis stabilization of gyroless and underactuated rigid spacecraft using modified rodrigues parameters," in *Proc. SICE Annu. Conf.*, Taipei, Taiwan, Aug. 2010, pp. 492–496.

[25] H.-H. Zhang, F. Wang, and P. M. Trivailo, "Spin-axis stabilisation of underactuated rigid spacecraft under sinusoidal disturbance," *Int. J. Control*, vol. 81, no. 12, pp. 1901–1909, Dec. 2008.
[26] Q. Zheng and F. Wu, "Nonlinear H_∞ control designs with axisymmetric spacecraft control," *J. Guid., Control, Dyn.*, vol. 32, no. 3, pp. 850–859, May 2009.
[27] H. Gui and G. Vukovich, "Robust adaptive spin-axis stabilization of a symmetric spacecraft using two bounded torques," *Adv. Space Res.*, vol. 56, no. 11, pp. 2495–2507, Dec. 2015.
[28] H. Rabiee, M. Ataei, and M. Ekramian, "Continuous nonsingular terminal sliding mode control based on adaptive sliding mode disturbance observer for uncertain nonlinear systems," *Automatica*, vol. 109, Nov. 2019, Art. no. 108515.
[29] B. Lu, Y. Fang, and N. Sun, "Continuous sliding mode control strategy for a class of nonlinear underactuated systems," *IEEE Trans. Autom. Control*, vol. 63, no. 10, pp. 3471–3478, Oct. 2018.
[30] J. Mendoza-Avila, J. A. Moreno, and L. M. Fridman, "Continuous twisting algorithm for third-order systems," *IEEE Trans. Autom. Control*, vol. 65, no. 7, pp. 2814–2825, Jul. 2020.
[31] P. M. Tiwari, S. Janardhanan, and M. un Nabi, "Rigid spacecraft attitude control using adaptive integral second order sliding mode," *Aerosp. Sci. Technol.*, vol. 42, pp. 50–57, Apr. 2015.
[32] Q. Shen, D. Wang, S. Zhu, and E. K. Poh, "Integral-type sliding mode fault-tolerant control for attitude stabilization of spacecraft," *IEEE Trans. Control Syst. Technol.*, vol. 23, no. 3, pp. 1131–1138, May 2015.
[33] H. Gui and G. Vukovich, "Adaptive fault-tolerant spacecraft attitude control using a novel integral terminal sliding mode," *Int. J. Robust Nonlinear Control*, vol. 27, no. 6, pp. 3174–3196, Jan. 2017.
[34] H. Gui and A. H. J. de Ruiter, "Adaptive fault-tolerant spacecraft pose tracking with control allocation," *IEEE Trans. Control Syst. Technol.*, vol. 27, no. 2, pp. 479–494, Mar. 2019.
[35] Y. Hong, J. Huang, and Y. Xu, "On an output feedback finite-time stabilization problem," *IEEE Trans. Autom. Control*, vol. 46, no. 2, pp. 305–309, 2001.
[36] P. Tsiotras and J. M. Longuski, "A new parameterization of the attitude kinematics," *J. Astron. Sci.*, vol. 43, no. 3, pp. 243–262, 1995.
[37] H. K. Khalil, *Nonlinear System*, 3rd ed. Upper Saddle River, NJ, USA: Prentice-Hall, 2002, pp. 303–334.

TAO WANG received the M.S. degree in aerospace science and technology from the Harbin Institute of Technology, Harbin, China, in 2011, where he is currently pursuing the Ph.D. degree. He is also a Senior Engineer with the China Academy of Space Technology, Beijing, China. His research interest includes spacecraft dynamics and control.

YINGCHUN ZHANG received the B.E. degree in automation from Tsinghua University, Beijing, China, in 1984, and the M.S. degree in control science and engineering from the Harbin Institute of Technology, Harbin, China, in 1987. He is currently a Professor with the Harbin Institute of Technology. His research interests include satellite fault diagnosis, fault tolerant control, and microsatellite design.